
A SIMPLE CONNECTION FROM LOSS FLATNESS TO COMPRESSED REPRESENTATIONS IN NEURAL NETWORKS

Shirui Chen

Department of Applied Mathematics
Computational Neuroscience Center
University of Washington
sc256@uw.edu

Stefano Recanatesi

Computational Neuroscience Center
Allen Institute
stefano.recanatesi@gmail.com

Eric Shea-Brown

Department of Applied Mathematics
Computational Neuroscience Center
University of Washington
Allen Institute
etsb@uw.edu

ABSTRACT

The generalization capacity of deep neural networks has been studied in a variety of ways, including at least two distinct categories of approach: one based on the shape of the loss landscape in parameter space, and the other based on the structure of the representation manifold in feature space (that is, in the space of unit activities). Although these two approaches are related, they are rarely studied together in an explicit connection. Here, we present a simple analysis that makes such a connection. We show that, in the last phase of learning of deep neural networks, compression of the manifold of neural representations correlates with the flatness of the loss around the minima explored by SGD. We show that this is predicted by a relatively simple mathematical relationship: a flatter loss corresponds to a lower upper-bound on the compression of neural representations. Our results closely build on the prior work of Ma and Ying, who demonstrated how flatness, characterized by small eigenvalues of the loss Hessian, develops in late learning phases and contributes to robustness against perturbations in network inputs. Moreover, we show a lack of a similarly direct connection between local dimensionality and sharpness, suggesting that this property may be controlled by different mechanisms than volume and hence may play a complementary role in neural representations. Overall, we advance a dual perspective on generalization in neural networks in both parameter and feature space.

1 INTRODUCTION

The remarkable capacity of deep neural networks to generalize has been studied in many ways. Generalization is a complex phenomenon influenced by numerous factors. These include model architecture, dataset size and diversity, and the specific task used to train a network. Researchers continue to develop new techniques to enhance generalization (Elsayed et al., 2018; Galanti et al., 2023). This is a vast field; however, from a theoretical point of view, we can identify two distinct categories of approach. These are works that study neural network generalization in the context of (a) the properties of minima of the loss function that learning algorithms find in parameter space (Dinh et al., 2017; Andriushchenko et al., 2023), and (b) the properties of the representations that optimized networks find in feature space (i.e., in the space of their neural activations) (Ben-Shaul & Dekel, 2022; Ben-Shaul et al., 2023; Rangamani et al., 2023).

In parameter space, both empirical studies and theoretical analyses have shown that deep neural networks often converge to flat and wide minima and that this can underlie their good generalization performance (e.g., (Ma & Ying, 2021; Blanc et al., 2020; Geiger et al., 2021; Li et al., 2022; Wu et al., 2018; Jastrzebski et al., 2018; Xie et al., 2021; Zhu et al., 2019)). Flat minima refer to regions in the loss landscape characterized by a relatively large basin, where the loss function doesn’t change much in different directions around the minimum. Elegant arguments show how models that converge to flat minima are more likely to generalize well (Yang et al., 2023). The intuition behind this is that in a flat minimum, small perturbations or noise in the input data are less likely to cause significant changes in the model’s output, resulting in improved robustness to variations in data from training to test.

In feature space, the phenomenon of compression (or neural collapse) refers to the observation that, as neural representations develop through the course of training, the activity patterns in both feed-forward and recurrent neural networks can become more compact and reside in lower-dimensional spaces (Farrell et al., 2022; Kothapalli et al., 2022; Zhu et al., 2021; Ansuini et al., 2019; Recanatani et al., 2019; Pappayan et al., 2020). This is closely related to the earlier information bottleneck ideas (Shwartz-Ziv & Tishby, 2017), which quantified allied effects via entropy. This phenomenon, which in many (but not all (Chizat et al., 2019; Flesch et al., 2022)) cases develops through training, can be enhanced by the architectural design of a network: for example, higher layers of a deep neural network usually have fewer neurons compared to the input layer, and autoencoders include internal “bottleneck layers” with significantly fewer neurons (Tishby & Zaslavsky, 2015).

Throughout, we focus on the second, or final, stage of learning, which proceeds after SGD has already found parameters that give near-optimal performance (i.e., zero training *error*) on the training data (Ma & Ying, 2021; Tishby & Zaslavsky, 2015; Ratzon et al., 2023). Here, additional learning still occurs, which changes the properties of the solutions in both feature and parameter space in very interesting ways.

Our work makes the following novel contributions:

- The paper identifies two representation space quantities that are bounded by sharpness – volume compression and maximum local sensitivity (MLS) – and gives new explicit formulas for these bounds that are reparametrization-invariant.
- The paper conducts empirical experiments with both VGG10 and MLP networks and finds that volume compression and MLS are indeed strongly correlated with sharpness.
- The paper finds that sharpness, volume compression, and MLS are also correlated, if more weakly, with test loss and hence generalization.

In these ways, we help reveal the interplay between key properties of trained neural networks in parameter space and representation space. Specifically, we identify a sequence of equality conditions for the bounds that link the volume and MLS of the neural representations to the sharpness in parameter space. These conditions help explain why there are mixed results on the relationship between sharpness and generalization in the literature, by looking through the additional lens of the induced representations. Our findings altogether suggest that allied views into representation space offer a valuable dual perspective to that of parameter space landscapes for understanding the effects of learning on generalization.

Our paper proceeds as follows. First, we review arguments of Ma & Ying (2021) that flatter minima can constrain the gradient of the loss with respect to network inputs and extend the formulation to the multidimensional input case (Sec. 2). Next, we prove that lower sharpness implies a lower upper bound on two metrics of the compression of the representation manifold in feature space: the local volume and the maximum local sensitivity (MLS) (Sec. 3.1, Sec. 3.2). We conclude our findings with simulations that confirm our central theoretical results and show how they can be applied in practice (Sec. 4).

2 BACKGROUND AND SETUP

Consider a feedforward neural network f with input data $\mathbf{x} \in \mathbb{R}^M$ and parameters $\boldsymbol{\theta}$. The output of the network is:

$$\mathbf{y} = f(\mathbf{x}; \boldsymbol{\theta}), \tag{1}$$

where $\mathbf{y} \in \mathbb{R}^N$ ($N < M$). We consider a quadratic loss $L(\mathbf{y}, \mathbf{y}_{\text{true}}) = \frac{1}{2} \|\mathbf{y} - \mathbf{y}_{\text{true}}\|^2$, a function of the outputs and ground truth \mathbf{y}_{true} . In the following, we will simply write $L(\mathbf{y})$, $L(f(\mathbf{x}, \boldsymbol{\theta}))$ or simply $L(\boldsymbol{\theta})$ to highlight the dependence of the loss on the output, the network or its parameters.

During the last phase of learning, Ma and colleagues have recently argued that SGD appears to regularize the sharpness of the loss (Li et al., 2022) (see also (Wu et al., 2018; Jastrzebski et al., 2018; Xie et al., 2021; Zhu et al., 2019)). This means that the dynamics of SGD lead network parameters to minima where the local loss landscape is flatter or wider. This is best captured by the sharpness, measured by the sum of the eigenvalues of the Hessian:

$$S(\boldsymbol{\theta}) = \text{Tr}(H), \quad (2)$$

with $H = \nabla^2 L(\boldsymbol{\theta})$ being the Hessian. A solution with low sharpness is a flatter solution. Following (Ma & Ying, 2021; Ratzon et al., 2023), we define $\boldsymbol{\theta}^*$ to be an “exact interpolation solution” on the zero training loss manifold in the parameter space (the zero loss manifold in what follows), where $f(\mathbf{x}_i, \boldsymbol{\theta}^*) = \mathbf{y}_i$ for all i ’s (with $i \in \{1..n\}$ indexing the training set) and $L(\boldsymbol{\theta}^*) = 0$. On the zero loss manifold, in particular, we have

$$S(\boldsymbol{\theta}^*) = \frac{1}{n} \sum_{i=1}^n \|\nabla_{\boldsymbol{\theta}} f(\mathbf{x}_i, \boldsymbol{\theta}^*)\|_F^2, \quad (3)$$

where $\|\cdot\|_F$ is the Frobenius norm. We give the proof of this equality in Appendix A. In practice, the parameter $\boldsymbol{\theta}$ will never reach an exact interpolation solution due to the gradient noise of SGD; however, Eq. (3) is a good enough approximation of the sharpness as long as we find an approximate interpolation solution (Lemma. A.1).

To see why minimizing the sharpness of the solution leads to more compressed representations, we need to move from the parameter space to the input space. To do so we review the argument of Ma & Ying (2021) that relates variations in the input data \mathbf{x} and input weights. Let \mathbf{W} be the input weights (the parameters of the first linear layer) of the network, and $\boldsymbol{\theta}$ be the rest of the parameters. Following (Ma & Ying, 2021), as the weights \mathbf{W} multiply the inputs \mathbf{x} , we have the following identities:

$$\begin{aligned} \|\nabla_{\mathbf{W}} f(\mathbf{W}\mathbf{x}; \bar{\boldsymbol{\theta}})\|_F &= \sqrt{\sum_{i,j,k} J_{jk}^2 x_i^2} = \|J\|_F \|\mathbf{x}\|_2 \geq \|J\|_2 \|\mathbf{x}\|_2, \\ \nabla_{\mathbf{x}} f(\mathbf{W}\mathbf{x}; \bar{\boldsymbol{\theta}}) &= \mathbf{W}^T J, \end{aligned} \quad (4)$$

where $J = \frac{\partial f(\mathbf{W}\mathbf{x}; \bar{\boldsymbol{\theta}})}{\partial (\mathbf{W}\mathbf{x})}$ is a complex expression as computed in, for example, backpropagation. From Eq. (4) and the sub-multiplicative property of the Frobenius norm and the matrix 2-norm, we have:

$$\begin{aligned} \|\nabla_{\mathbf{x}} f(\mathbf{W}\mathbf{x}; \bar{\boldsymbol{\theta}})\|_F &\leq \frac{\|\mathbf{W}\|_F}{\|\mathbf{x}\|_2} \|\nabla_{\mathbf{W}} f(\mathbf{W}\mathbf{x}; \bar{\boldsymbol{\theta}})\|_F, \\ \|\nabla_{\mathbf{x}} f(\mathbf{W}\mathbf{x}; \bar{\boldsymbol{\theta}})\|_2 &\leq \frac{\|\mathbf{W}\|_2}{\|\mathbf{x}\|_2} \|\nabla_{\mathbf{W}} f(\mathbf{W}\mathbf{x}; \bar{\boldsymbol{\theta}})\|_F. \end{aligned} \quad (5)$$

If the norms $\|\mathbf{W}\|_F$ or $\|\mathbf{W}\|_2$ and $\|\mathbf{x}\|_2$ are not excessively large or small, respectively, these bounds control the gradient with respect to inputs via the gradient with respect to weights. This in turn reveals the impact of flatness in the loss function:

$$\begin{aligned} \frac{1}{n} \sum_{i=1}^n \|\nabla_{\mathbf{x}} f(\mathbf{x}_i, \boldsymbol{\theta}^*)\|_F^k &\leq \frac{\|\mathbf{W}\|_F^k}{\min_i \|\mathbf{x}_i\|_2^k} \frac{1}{n} \sum_{i=1}^n \|\nabla_{\mathbf{W}} f(\mathbf{x}_i, \boldsymbol{\theta}^*)\|_F^k \\ &\leq \frac{\|\mathbf{W}\|_F^k}{\min_i \|\mathbf{x}_i\|_2^k} \frac{1}{n} \sum_{i=1}^n \|\nabla_{\boldsymbol{\theta}} f(\mathbf{x}_i, \boldsymbol{\theta}^*)\|_F^k. \end{aligned} \quad (6)$$

We define $G := \frac{1}{n} \sum_{i=1}^n \|\nabla_{\mathbf{x}} f(\mathbf{x}_i, \boldsymbol{\theta}^*)\|_F^2$ when $k = 2$. Similarly,

$$\frac{1}{n} \sum_{i=1}^n \|\nabla_{\mathbf{x}} f(\mathbf{x}_i, \boldsymbol{\theta}^*)\|_2^k \leq \frac{\|\mathbf{W}\|_2^k}{\min_i \|\mathbf{x}_i\|_2^k} \frac{1}{n} \sum_{i=1}^n \|\nabla_{\boldsymbol{\theta}} f(\mathbf{x}_i, \boldsymbol{\theta}^*)\|_F^k. \quad (7)$$

Thus, in (Ma & Ying, 2021), the effect of input perturbations is constrained by the sharpness of the loss function. The flatter the minimum of the loss, the lower the effect of input space perturbations on the network function $f(\mathbf{x}, \boldsymbol{\theta}^*)$ as determined by gradients.

3 FROM ROBUSTNESS TO INPUTS TO COMPRESSION OF REPRESENTATIONS

We now further analyze variations in the input and how they propagate through the network to shape representations of sets of inputs. Although we only study the representations of the output of the network here, our results apply to representations of any middle layer by defining f to be the transformation from input to the middle layer of interest. Overall, we focus on three key metrics of network representations: local dimensionality, volumetric ratio, and maximum local sensitivity. These quantities enable us to establish and evaluate the influence of input variations and, in turn, sharpness on neural representation properties.

3.1 WHY SHARPNESS BOUNDS LOCAL VOLUMETRIC TRANSFORMATION IN REPRESENTATION SPACE

Consider an input data point $\bar{\mathbf{x}}$ drawn from the training set: $\bar{\mathbf{x}} = \mathbf{x}_i$ for a specific $i \in \{1..n\}$. Let the set of all possible perturbations around $\bar{\mathbf{x}}$ in the input space be the ball $\mathcal{B}(\bar{\mathbf{x}})_\alpha \sim \mathcal{N}(\bar{\mathbf{x}}, \alpha \mathcal{I})$, where α depends on the perturbation’s covariance, which is given as $C_{\mathcal{B}(\bar{\mathbf{x}})} = \alpha \mathcal{I}$, with \mathcal{I} as the identity matrix. We’ll explore the network’s representation of inputs by measuring the expansion or contraction of the ball $\mathcal{B}(\bar{\mathbf{x}})_\alpha$ as it propagates through the network. We first propagate the ball through the network transforming each point \mathbf{x} into its corresponding image $f(\mathbf{x})$. Following a Taylor expansion for points within $\mathcal{B}(\bar{\mathbf{x}})_\alpha$ as $\alpha \rightarrow 0$ we have:

$$f(\mathbf{x}) = f(\bar{\mathbf{x}}) + \nabla_{\mathbf{x}}(f(\bar{\mathbf{x}}, \boldsymbol{\theta}^*))(\mathbf{x} - \bar{\mathbf{x}}). \quad (8)$$

We can express the limit of the covariance matrix $C_{f(\mathcal{B}(\bar{\mathbf{x}})_\alpha)}$ of the output $f(\mathbf{x})$ as

$$C_f^{\text{lim}} := \lim_{\alpha \rightarrow 0} C_{f(\mathcal{B}(\bar{\mathbf{x}})_\alpha)} = \alpha \nabla_{\mathbf{x}} f(\bar{\mathbf{x}}, \boldsymbol{\theta}^*) \nabla_{\mathbf{x}}^T f(\bar{\mathbf{x}}, \boldsymbol{\theta}^*). \quad (9)$$

Our covariance expressions capture the distribution of points in $\mathcal{B}(\bar{\mathbf{x}})_\alpha$ as they go through the network $f(\bar{\mathbf{x}}, \boldsymbol{\theta}^*)$.

Now we quantify how a network compresses its input volumes via the local volumetric ratio, between a hypercube of side length h at \mathbf{x} and its image under transformation f :

$$\begin{aligned} d\text{Vol}^{\text{ratio}}|_{f(\mathbf{x}, \boldsymbol{\theta}^*)} &= \lim_{h \rightarrow 0} \frac{\text{Vol}(f(\mathbf{x}, \boldsymbol{\theta}^*))}{\text{Vol}(\mathbf{x})} \\ &= \sqrt{\det(\nabla_{\mathbf{x}} f^T \nabla_{\mathbf{x}} f)}, \end{aligned} \quad (10)$$

which is equal to the square root of the product of all positive eigenvalues of C_f^{lim} . Exploiting the bound on the gradients derived earlier in Eq. (5), we derive a similar bound for the volumetric ratio:

$$\begin{aligned} d\text{Vol}^{\text{ratio}}|_{f(\mathbf{x}, \boldsymbol{\theta}^*)} &\leq \left(\frac{\text{Tr} \nabla_{\mathbf{x}} f^T \nabla_{\mathbf{x}} f}{N} \right)^{N/2} \\ &= N^{-N/2} \|\nabla_{\mathbf{x}} f(\mathbf{x}, \boldsymbol{\theta}^*)\|_F^N, \end{aligned} \quad (11)$$

where the first line uses the inequality between arithmetic and geometric means and the second the definition of the Frobenius norm. By introducing the averaged volumetric ratio across all input points $dV^{\text{ratio}}(\boldsymbol{\theta}^*) = \frac{1}{n} \sum_{i=1}^n d\text{Vol}^{\text{ratio}}|_{f(\mathbf{x}_i, \boldsymbol{\theta}^*)}$, we obtain:

$$dV^{\text{ratio}}(\boldsymbol{\theta}^*) \leq \frac{N^{-N/2}}{n} \sum_{i=1}^n \|\nabla_{\mathbf{x}} f(\mathbf{x}_i, \boldsymbol{\theta}^*)\|_F^N \leq \frac{n^{\max(N/2-1, 0)} \|\mathbf{W}\|_F^N}{\min_i \|\mathbf{x}_i\|_2^N} \left(\frac{S(\boldsymbol{\theta}^*)}{N} \right)^{N/2} \quad (12)$$

for all $N \geq 1$. A detailed derivation of the above inequality is given in Appendix B. Eq. (12) implies that flattened minima of the loss function in parameter space contribute to the compression of the data’s representation manifold. Our analysis demonstrates that the robustness properties of the network link these two phenomena to input perturbations.

3.2 MAXIMUM LOCAL SENSITIVITY AS AN ALLIED METRIC TO TRACK NEURAL REPRESENTATION GEOMETRY

We observe that the equality condition in the first line of Eq. (11) rarely holds in practice, since to achieve equality, we need all singular values of the Jacobian matrix $\nabla_{\mathbf{x}} f$ to be identical. Our experiments in Sec. 4 show that the local dimensionality decreases rapidly with training onset, indicating

that $\nabla_{\mathbf{x}} f^T \nabla_{\mathbf{x}} f$ has a non-uniform eigenspectrum. Moreover, the volume will decrease rapidly as the smallest eigenvalue vanishes. Thus, although sharpness upper bounds the volumetric ratio, it does not correlate well with it, nor does the volumetric ratio give an accurate estimate of sharpness. Fortunately, considering only the maximum eigenvalue instead of the product alleviates this problem (recall that $\det(\nabla_{\mathbf{x}} f^T \nabla_{\mathbf{x}} f)$ in the definition Eq. (10) or volumetric ratio is the product of all eigenvalues): we define the maximum local sensitivity (MLS) to be the largest singular value of $\nabla_{\mathbf{x}} f$. The MLS is equivalently the matrix 2-norm of $\nabla_{\mathbf{x}} f$. Intuitively, it is the largest possible local change of $f(\mathbf{x})$ when the norm of the perturbation to \mathbf{x} is regularized. We denote the sample mean of MLS as $\overline{\text{MLS}}$. Given this definition, we obtain a bound on MLS using the Frobenius norm of the first linear layer, the quadratic mean of the input norm, and the sharpness:

$$\overline{\text{MLS}} = \frac{1}{n} \sum_{i=1}^n \|\nabla_{\mathbf{x}} f(\mathbf{x}_i, \theta^*)\|_2 \leq \|\mathbf{W}\|_2 \sqrt{\frac{1}{n} \sum_{i=1}^n \frac{1}{\|\mathbf{x}_i\|_2^2}} S(\theta^*)^{1/2}. \quad (13)$$

The derivation of the above bound is included in Appendix C, where we use the Cauchy-Schwarz inequality to tighten the bound in Eq. (7). As an alternative measure of compressed representations, we empirically show in Appendix D.2 that MLS has a higher correlation with sharpness and test loss than the other two measures we consider in the feature space. We include more analysis of the tightness of this bound in Appendix D and discuss its connection to other works therein.

3.3 LOCAL DIMENSIONALITY IS TIED TO, BUT NOT BOUNDED BY, SHARPNESS

Now we introduce a local measure of dimensionality based on this covariance, the local Participation Ratio, given by:

$$D_{\text{PR}}(f(\bar{\mathbf{x}})) = \lim_{\alpha \rightarrow 0} \frac{\text{Tr}[C_f(\mathcal{B}(\mathbf{x}))]^2}{\text{Tr}[(C_f(\mathcal{B}(\mathbf{x})))^2]} = \frac{\text{Tr}[C_f^{\text{lim}}]^2}{\text{Tr}[(C_f^{\text{lim}})^2]} \quad (14)$$

(cf. (Gao et al., 2017; Litwin-Kumar et al., 2017; Recanatesi et al., 2022)). This quantity can be averaged across a set of samples: $D_{\text{PR}}(\theta^*) = \frac{1}{n} \sum_{i=1}^n D_{\text{PR}}(f(\mathbf{x}_i))$. This quantity in some sense represents the sparseness of the eigenvalues of C_f^{lim} : if we let $\boldsymbol{\lambda}$ be all the eigenvalues of C_f^{lim} , then the local dimensionality can be written as $D_{\text{PR}} = (\|\boldsymbol{\lambda}\|_1 / \|\boldsymbol{\lambda}\|_2)^2$, which attains its maximum value when all eigenvalues are equal to each other, and its minimum when all eigenvalues except for the leading one are zero. Note that the quantity retains the same value when $\boldsymbol{\lambda}$ is arbitrarily scaled, therefore it is hard to find a relationship between local dimensionality and $\|\nabla_{\mathbf{x}} f(\mathbf{x}, \theta^*)\|_F^2$, which is basically $\|\boldsymbol{\lambda}\|_1$.

4 EXPERIMENTS

4.1 SHARPNESS AND COMPRESSION: VERIFYING THE THEORY

The theoretical results derived above show that, during the later phase of training – the interpolation phase – measures of compression of the network’s representation are upper bounded by a function of the sharpness of the loss function in parameter space. This links sharpness and representation compression: the flatter the loss landscape, the lower the upper bound on the representation’s compression metrics.

However, it remains to be tested in practice whether these bounds are sufficiently tight to show a clear relationship between sharpness and representation collapse. For one such test, we conducted the following experiment. We trained a network (Simonyan & Zisserman, 2015) to classify images from the CIFAR-10 dataset and calculated the sharpness (Eq. (2)), the log volumetric ratio (Eq. (10)), and the left-hand side of Eq. (6) (the gradient with respect to the inputs, a quantity we term G in the figures below) during the training phase (Fig 1 and 2). We trained the network (VGG10) using SGD on images from 2 classes (out of 10) so that convergence to the interpolation regime, i.e. zero error, was faster. We explored the influence of two specific parameters that have a substantial effect on the network’s training: learning rate and batch size. For each pair of learning rate and batch size parameters, we computed all quantities at hand across 100 input samples and five different random initializations for network weights.

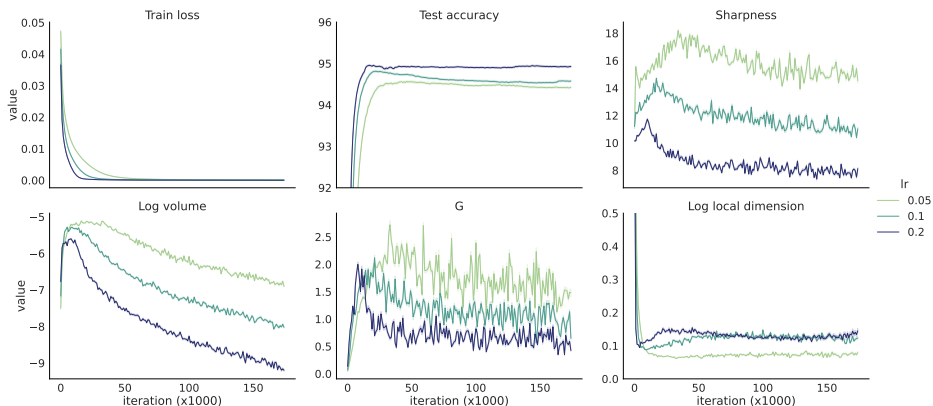


Figure 1: Trends in key variables across SGD training of the VGG10 network with fixed batch size (equal to 20) and varying learning rates (0.05, 0.1 and 0.2). After the loss is minimized (so that an approximate interpolation solution is found) sharpness and volumes decrease together. Moreover, higher learning rates lead to lower sharpness and hence stronger compression. From left to right: train loss, test accuracy, sharpness (square root of Eq. (3)), log volumetric ratio (Eq. (10)), left-hand side of Eq. (6) with $k = 2$ (axes titled G), and local dimensionality of the network output (Eq. (14)).

In the first set of experiments, we studied the link between a decrease in sharpness during the latter phases of training and volume compression (Fig. 1). We noticed that when the network reaches the interpolation regime, and the sharpness decreases, so does the volume. Similarly, the quantity G decreases. All these results were consistent across multiple learning rates for a fixed batch size (of 20): specifically, for learning rates that yielded lower values of sharpness, volume was lower as well.

We then repeated the experiments while keeping the learning rate fixed ($lr=0.1$) and varying the batch size. The same broadly consistent trends emerged, linking a decrease in the sharpness to a compression in the representation volume (Fig. 2). However, we also found that while sharpness stops decreasing after about $50 \cdot 10^3$ iterations for a batch size of 32, the volume continues to decrease as learning proceeds. This suggests that other mechanisms, beyond sharpness, may be at play in driving the compression of volumes.

We repeat the experiments with an MLP trained on the FashionMNIST dataset (Fig. E.8 and Fig. E.7). Although the sharpness does not noticeably decrease towards the end of the training, it follows the same trend as G , consistent with our bound. The volume continues to decrease after the sharpness plateaus, albeit at a much slower rate, again matching our theory while suggesting that an additional factor may be involved in its decrease.

4.2 SHARPNESS AND COMPRESSION ON TEST SET DATA

Even though Eq. (3) is exact for interpolation solutions only (i.e., those with zero loss), we found that the test loss is small enough (Fig. 3) so that it should be a good approximation for test data as well. Therefore we analyzed our simulations to study trends in sharpness and volume for these held-out test data as well (Fig. 3). We discovered that this sharpness increased rather than diminished as a result of training. We hypothesized that sharpness could correlate with the difficulty of classifying testing points. This was supported by the fact that the sharpness of misclassified test data was even greater than that of all test data. Again we see that G has the same trend as the sharpness. Despite this increase in sharpness, the volume followed the same pattern as the training set. This suggests that compression in representation space is a robust phenomenon that can be driven by additional phenomena beyond sharpness. Nevertheless, the compression still is weaker for misclassified test samples that have higher sharpness than other test samples. Overall, these results emphasize an interesting distinction between how sharpness evolves for training vs. test data.

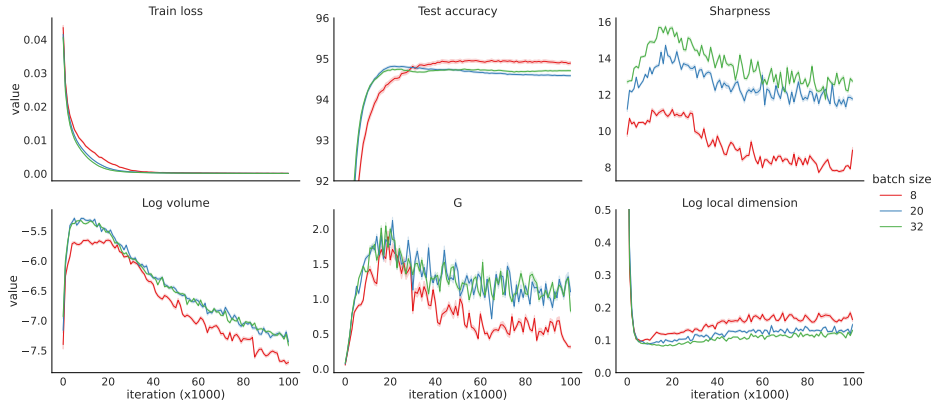


Figure 2: Trends in key variables across SGD training of the VGG10 network with fixed learning rate size (equal to 0.1) and varying batch size (8, 20, and 32). After the loss is minimized (so that an interpolation solution is found) sharpness and volumes decrease together. Moreover, lower batch sizes lead to lower sharpness and hence stronger compression. From left to right in row-wise order: train loss, test accuracy, sharpness (square root of Eq. (3)), log volumetric ratio (Eq. (10)), left-hand side of Eq. (6) with $k = 2$ (axes titled G), and local dimensionality of the network output (Eq. (14)).

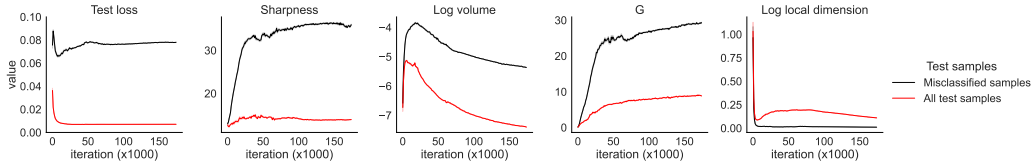


Figure 3: Trends in key variables across SGD training of the VGG10 network with fixed learning rate (equal to 0.1) and batch size (equal to 20) for samples of the test set. After the loss is minimized, we compute sharpness and volume on the test set. Moreover, the same quantities are computed separately over the entire test set or only on samples that are misclassified. In order from left to right in row-wise order: train loss, test loss, sharpness (Eq. (2)), log volumetric ratio (Eq. (10)), left-hand side of Eq. (6) with $k = 2$ (axes titled G), and local dimensionality of the network output (Eq. (14)).

4.3 SHARPNESS AND LOCAL DIMENSIONALITY

Lastly, we analyze the representation’s local dimensionality in a manner analogous to the analysis of volume and MLS. A priori, it is ambiguous whether the dimensionality of the data representation should increase or decrease as the volume is compressed. For instance, the volume could decrease while maintaining its overall form and symmetry, thus preserving its dimensionality. Alternatively, one or more of the directions in the relevant tangent space could be selectively compressed, leading to an overall reduction in dimensionality.

Figures 1 and 2 show our experiments computing the local dimensionality over the course of learning. Here, we find that the local dimensionality of the representation decreases as the loss decreases to near 0, which is consistent with the viewpoint that the network compresses representations in feature space as much as possible, retaining only the directions that code for task-relevant features (Berner et al., 2020; Cohen et al., 2020). However, the local dimensionality exhibits unpredictable behavior that cannot be explained by the sharpness once the network is near the zero-loss manifold and training continues. This discrepancy is consistent with the bounds established by our theory, which only bound the numerator of Eq. (14). It is also consistent with the property of local dimensionality that we described in Sec. 3.3 overall: it encodes the sparseness of the eigenvalues but it does not encode the magnitude of them. This shows how local dimensionality is a distinct quality of network representations compared with volume, and is driven by mechanisms that differ from sharpness alone. We emphasize that the dimensionality we study here is a local measure, on the finest scale around a point on the “global” manifold of unit activities; dimension on larger scales

(i.e., across categories or large sets of task inputs (Farrell et al., 2022; Gao et al., 2017)) may show different trends.

5 CONCLUSION

This work presents a dual perspective, uniting views in both parameter and in feature space, of several key properties of trained neural networks that have been linked to their ability to generalize. We identify two representation space quantities that are bounded by sharpness – volume compression and maximum local sensitivity – and give new explicit formulas for these bounds. We conduct experiments with both VGG10 and MLP networks and find that the predictions of these bounds are born out for these networks, illustrating how MLS in particular is strongly correlated with sharpness. We also establish that sharpness, volume compression, and MLS are correlated, if more weakly, with test loss and hence generalization. Overall, we establish explicit links between sharpness properties in parameter spaces and compression and robustness properties in representation space.

By demonstrating both how these links can be tight, and how and when they may also become loose, we show that taking this dual perspective can bring more clarity to the often confusing question of what quantifies how well a network will generalize in practice. Indeed, many works, as reviewed in the introduction, have demonstrated how sharpness in parameter space can lead to generalization, but recent studies have established contradictory results. We show how looking at quantities not only in the parameter space (sharpness), but also in the feature space (compression, maximum local sensitivity, etc.) may help explain the wide range of results.

This said, we view our study as a starting point to open doors between two often-distinct perspectives on generalization in neural networks. Additional theoretical and experimental research is warranted to systematically investigate the implications of our findings, with a key area being further learning problems, such as predictive learning, beyond the classification tasks studied here. Nevertheless, we are confident that highly interesting and clarifying findings lie ahead at the interface between the parameter and representation space quantities explored here.

REFERENCES

- Maksym Andriushchenko, Francesco Croce, Maximilian Müller, Matthias Hein, and Nicolas Flammarion. A modern look at the relationship between sharpness and generalization. *arXiv preprint arXiv:2302.07011*, 2023.
- Alessio Ansuini, Alessandro Laio, Jakob H. Macke, and Davide Zoccolan. Intrinsic dimension of data representations in deep neural networks. *Advances in Neural Information Processing Systems*, 32, 2019.
- Ido Ben-Shaul and Shai Dekel. Nearest class-center simplification through intermediate layers. In *Topological, Algebraic and Geometric Learning Workshops 2022*, pp. 37–47. PMLR, 2022.
- Ido Ben-Shaul, Ravid Shwartz-Ziv, Tomer Galanti, Shai Dekel, and Yann LeCun. Reverse engineering self-supervised learning. *arXiv preprint arXiv:2305.15614*, 2023.
- Julius Berner, Philipp Grohs, and Arnulf Jentzen. Analysis of the generalization error: Empirical risk minimization over deep artificial neural networks overcomes the curse of dimensionality in the numerical approximation of black–scholes partial differential equations. *SIAM Journal on Mathematics of Data Science*, 2(3):631–657, 2020. Publisher: SIAM.
- Guy Blanc, Neha Gupta, Gregory Valiant, and Paul Valiant. Implicit regularization for deep neural networks driven by an ornstein-uhlenbeck like process, 2020. URL <http://arxiv.org/abs/1904.09080>.
- Lenaïc Chizat, Edouard Oyallon, and Francis Bach. On lazy training in differentiable programming. *Advances in neural information processing systems*, 32, 2019.
- Uri Cohen, SueYeon Chung, Daniel D. Lee, and Haim Sompolinsky. Separability and geometry of object manifolds in deep neural networks. *Nature communications*, 11(1):746, 2020. Publisher: Nature Publishing Group UK London.

-
- Lijun Ding, Dmitriy Drusvyatskiy, Maryam Fazel, and Zaid Harchaoui. Flat minima generalize for low-rank matrix recovery, 2023.
- Laurent Dinh, Razvan Pascanu, Samy Bengio, and Yoshua Bengio. Sharp minima can generalize for deep nets. In *International Conference on Machine Learning*, pp. 1019–1028. PMLR, 2017.
- Gamaleldin Elsayed, Dilip Krishnan, Hossein Mobahi, Kevin Regan, and Samy Bengio. Large margin deep networks for classification. *Advances in neural information processing systems*, 31, 2018.
- Matthew Farrell, Stefano Recanatesi, Timothy Moore, Guillaume Lajoie, and Eric Shea-Brown. Gradient-based learning drives robust representations in recurrent neural networks by balancing compression and expansion. *Nature Machine Intelligence*, 4(6):564–573, 2022. Publisher: Nature Publishing Group UK London.
- Timo Flesch, Keno Juechems, Tsvetomira Dumbalska, Andrew Saxe, and Christopher Summerfield. Orthogonal representations for robust context-dependent task performance in brains and neural networks. *Neuron*, 110(7):1258–1270, 2022.
- Tomer Galanti, Liane Galanti, and Ido Ben-Shaul. Comparative generalization bounds for deep neural networks. *Transactions on Machine Learning Research*, 2023.
- Peiran Gao, Eric Trautmann, Byron Yu, Gopal Santhanam, Stephen Ryu, Krishna Shenoy, and Surya Ganguli. A theory of multineuronal dimensionality, dynamics and measurement. *BioRxiv*, pp. 214262, 2017.
- Khashayar Gatmiry, Zhiyuan Li, Ching-Yao Chuang, Sashank Reddi, Tengyu Ma, and Stefanie Jegelka. The inductive bias of flatness regularization for deep matrix factorization, 2023.
- Mario Geiger, Leonardo Petrini, and Matthieu Wyart. Landscape and training regimes in deep learning. *Physics Reports*, 924:1–18, 2021. ISSN 0370-1573. doi: 10.1016/j.physrep.2021.04.001. URL <https://www.sciencedirect.com/science/article/pii/S0370157321001290>.
- Stanisław Jastrzebski, Zachary Kenton, Devansh Arpit, Nicolas Ballas, Asja Fischer, Yoshua Bengio, and Amos Storkey. Three Factors Influencing Minima in SGD, September 2018. URL <http://arxiv.org/abs/1711.04623>. arXiv:1711.04623 [cs, stat].
- Vignesh Kothapalli, Ebrahim Rasromani, and Vasudev Awatramani. Neural collapse: A review on modelling principles and generalization. *arXiv preprint arXiv:2206.04041*, 2022.
- Zhiyuan Li, Tianhao Wang, and Sanjeev Arora. What happens after SGD reaches zero loss? – a mathematical framework, 2022. URL <http://arxiv.org/abs/2110.06914>.
- Ashok Litwin-Kumar, Kameron Decker Harris, Richard Axel, Haim Sompolinsky, and LF Abbott. Optimal degrees of synaptic connectivity. *Neuron*, 93(5):1153–1164, 2017.
- Chao Ma and Lexing Ying. On linear stability of SGD and input-smoothness of neural networks, 2021. URL <http://arxiv.org/abs/2105.13462>.
- Mor Shpigel Nacson, Kavya Ravichandran, Nathan Srebro, and Daniel Soudry. Implicit bias of the step size in linear diagonal neural networks. In Kamalika Chaudhuri, Stefanie Jegelka, Le Song, Csaba Szepesvari, Gang Niu, and Sivan Sabato (eds.), *Proceedings of the 39th International Conference on Machine Learning*, volume 162 of *Proceedings of Machine Learning Research*, pp. 16270–16295. PMLR, 17–23 Jul 2022. URL <https://proceedings.mlr.press/v162/nacson22a.html>.
- Vardan Papyan, XY Han, and David L Donoho. Prevalence of neural collapse during the terminal phase of deep learning training. *Proceedings of the National Academy of Sciences*, 117(40):24652–24663, 2020.
- Akshay Rangamani, Marius Lindgaard, Tomer Galanti, and Tomaso A Poggio. Feature learning in deep classifiers through intermediate neural collapse. In *International Conference on Machine Learning*, pp. 28729–28745. PMLR, 2023.

-
- Aviv Ratzon, Dori Derdikman, and Omri Barak. Representational drift as a result of implicit regularization, 2023. URL <https://www.biorxiv.org/content/10.1101/2023.05.04.539512v3>. Pages: 2023.05.04.539512 Section: New Results.
- Stefano Recanatesi, Matthew Farrell, Madhu Advani, Timothy Moore, Guillaume Lajoie, and Eric Shea-Brown. Dimensionality compression and expansion in deep neural networks. *arXiv preprint arXiv:1906.00443*, 2019.
- Stefano Recanatesi, Serena Bradde, Vijay Balasubramanian, Nicholas A Steinmetz, and Eric Shea-Brown. A scale-dependent measure of system dimensionality. *Patterns*, 3(8), 2022.
- Ravid Shwartz-Ziv and Naftali Tishby. Opening the black box of deep neural networks via information. *arXiv preprint arXiv:1703.00810*, 2017.
- Karen Simonyan and Andrew Zisserman. Very deep convolutional networks for large-scale image recognition, 2015.
- Naftali Tishby and Noga Zaslavsky. Deep learning and the information bottleneck principle, 2015. URL <http://arxiv.org/abs/1503.02406>.
- Kaiyue Wen, Zhiyuan Li, and Tengyu Ma. Sharpness minimization algorithms do not only minimize sharpness to achieve better generalization, 2023.
- Lei Wu, Chao Ma, and Weinan E. How SGD Selects the Global Minima in Over-parameterized Learning: A Dynamical Stability Perspective. In *Advances in Neural Information Processing Systems*, volume 31. Curran Associates, Inc., 2018. URL https://papers.nips.cc/paper_files/paper/2018/hash/6651526b6fb8f29a00507de6a49ce30f-Abstract.html.
- Zeke Xie, Issei Sato, and Masashi Sugiyama. A Diffusion Theory For Deep Learning Dynamics: Stochastic Gradient Descent Exponentially Favors Flat Minima, January 2021. URL <http://arxiv.org/abs/2002.03495>. arXiv:2002.03495 [cs, stat].
- Ning Yang, Chao Tang, and Yuhai Tu. Stochastic gradient descent introduces an effective landscape-dependent regularization favoring flat solutions. *Physical Review Letters*, 130(23):237101, 2023. doi: 10.1103/PhysRevLett.130.237101. URL <https://link.aps.org/doi/10.1103/PhysRevLett.130.237101>. Publisher: American Physical Society.
- Zhanxing Zhu, Jingfeng Wu, Bing Yu, Lei Wu, and Jinwen Ma. The Anisotropic Noise in Stochastic Gradient Descent: Its Behavior of Escaping from Sharp Minima and Regularization Effects, June 2019. URL <http://arxiv.org/abs/1803.00195>. arXiv:1803.00195 [cs, stat].
- Zhihui Zhu, Tianyu Ding, Jinxin Zhou, Xiao Li, Chong You, Jeremias Sulam, and Qing Qu. A geometric analysis of neural collapse with unconstrained features. *Advances in Neural Information Processing Systems*, 34:29820–29834, 2021.

A PROOF OF EQ. (3)

Lemma A.1. *If θ is an approximate interpolation solution, i.e. $\|f(\mathbf{x}_i, \theta) - \mathbf{y}_i\| < \varepsilon$ for $i \in \{1, 2, \dots, n\}$, and second derivatives of the network function $\|\nabla_{\theta_j^2} f(\mathbf{x}_i, \theta)\| < M$ is bounded, then*

$$S(\theta^*) = \frac{1}{n} \sum_{i=1}^n \|\nabla_{\theta} f(\mathbf{x}_i, \theta^*)\|_F^2 + O(\varepsilon) \quad (15)$$

Proof. Using basic calculus we get

$$\begin{aligned} S(\theta) &= \text{Tr}(\nabla^2 L(\theta)) \\ &= \frac{1}{2n} \sum_{i=1}^n \text{Tr}(\nabla_{\theta}^2 \|f(\mathbf{x}_i, \theta) - \mathbf{y}_i\|^2) \\ &= \frac{1}{2n} \sum_{i=1}^n \text{Tr} \nabla_{\theta} (2(f(\mathbf{x}_i, \theta) - \mathbf{y}_i)^T \nabla_{\theta} f(\mathbf{x}_i, \theta)) \\ &= \frac{1}{n} \sum_{i=1}^n \sum_{j=1}^m \frac{\partial}{\partial \theta_j} ((f(\mathbf{x}_i, \theta) - \mathbf{y}_i)^T \nabla_{\theta} f(\mathbf{x}_i, \theta))_j \\ &= \frac{1}{n} \sum_{i=1}^n \sum_{j=1}^m \frac{\partial}{\partial \theta_j} (f(\mathbf{x}_i, \theta) - \mathbf{y}_i)^T \nabla_{\theta_j} f(\mathbf{x}_i, \theta) \\ &= \frac{1}{n} \sum_{i=1}^n \sum_{j=1}^m \|\nabla_{\theta_j} f(\mathbf{x}_i, \theta)\|_2^2 + (f(\mathbf{x}_i, \theta) - \mathbf{y}_i)^T \nabla_{\theta_j^2} f(\mathbf{x}_i, \theta) \\ &= \frac{1}{n} \sum_{i=1}^n \|\nabla_{\theta} f(\mathbf{x}_i, \theta)\|_F^2 + \frac{1}{n} \sum_{i=1}^n (f(\mathbf{x}_i, \theta) - \mathbf{y}_i)^T \nabla_{\theta_j^2} f(\mathbf{x}_i, \theta). \end{aligned}$$

Therefore

$$\left| S(\theta) - \frac{1}{n} \sum_{i=1}^n \|\nabla_{\theta} f(\mathbf{x}_i, \theta)\|_F^2 \right| < \frac{1}{n} \sum_{i=1}^n |(f(\mathbf{x}_i, \theta) - \mathbf{y}_i)^T \nabla_{\theta_j^2} f(\mathbf{x}_i, \theta)| < M\varepsilon = O(\varepsilon). \quad (16)$$

□

In other words, when the network reaches zero training error and enters the interpolation phase (i.e. it classifies all training data correctly), Eq. (3) will be a good enough approximation of the sharpness because the quadratic training loss is sufficiently small.

B PROOF OF EQ. (12)

We first show that Eq. (6) is correct. Because of Eq. (5), we have the first inequality of Eq. (6),

$$\begin{aligned} \frac{1}{n} \sum_{i=1}^n \|\nabla_{\mathbf{x}} f(\mathbf{x}_i, \theta^*)\|_F^k &\leq \|\mathbf{W}\|_F^k \frac{1}{n} \sum_{i=1}^n \frac{\|\nabla_{\mathbf{w}} f(\mathbf{x}_i, \theta^*)\|_F^k}{\|\mathbf{x}_i\|_2^k} \\ &\leq \frac{\|\mathbf{W}\|_F^k}{\min_i \|\mathbf{x}_i\|_2^k} \frac{1}{n} \sum_{i=1}^n \|\nabla_{\mathbf{w}} f(\mathbf{x}_i, \theta^*)\|_F^k. \end{aligned} \quad (17)$$

Since the input weights \mathbf{W} is just a part of all the weights (θ) of the network, we have $\|\nabla_{\mathbf{w}} f(\mathbf{x}_i, \theta^*)\|_F^k \leq \|\nabla_{\theta} f(\mathbf{x}_i, \theta^*)\|_F^k$. Therefore

$$\frac{\|\mathbf{W}\|_F^k}{\min_i \|\mathbf{x}_i\|_2^k} \frac{1}{n} \sum_{i=1}^n \|\nabla_{\mathbf{w}} f(\mathbf{x}_i, \theta^*)\|_F^k \leq \frac{\|\mathbf{W}\|_F^k}{\min_i \|\mathbf{x}_i\|_2^k} \frac{1}{n} \sum_{i=1}^n \|\nabla_{\theta} f(\mathbf{x}_i, \theta^*)\|_F^k. \quad (18)$$

To show the correctness of Eq. (12), we discuss two cases.

Case 1: $k \geq 2$

Lemma B.1. For vector \mathbf{x} , $\|\mathbf{x}\|_p \geq \|\mathbf{x}\|_q$ for $1 \leq p \leq q \leq \infty$.

Proof. First we show that for $0 < k < 1$, we have $(|a| + |b|)^k \leq |a|^k + |b|^k$. It's trivial when either a or b is 0. So W.L.O.G, we can assume that $|a| < |b|$, and divide both sides by $|b|^k$. Therefore it suffices to show that for $0 < t < 1$, $(1+t)^k < t^k + 1$. Let $f(t) = (1+t)^k - t^k - 1$, then $f(0) = 0$, and $f'(t) = k(1+t)^{k-1} - kt^{k-1}$. Because $k-1 < 0$, $1+t > 1$ and $t < 1$, $t^{k-1} > (1+t)^{k-1}$. Therefore $f'(t) < 0$ and $f(t) < 0$ for $0 < t < 1$. Combining all cases, we have $(|a| + |b|)^k \leq |a|^k + |b|^k$ for $0 < k < 1$. By induction, we have $(\sum_n |a_n|)^k \leq \sum_n |a_n|^k$.

Now we can prove the lemma using the conclusion above,

$$\left(\sum_n |x_n|^q \right)^{1/q} = \left(\sum_n |x_n|^q \right)^{p/q \cdot 1/p} \leq \left(\sum_n (|x_n|^q)^{p/q} \right)^{1/p} = \left(\sum_n |x_n|^p \right)^{1/p} \quad (19)$$

□

Now take the x_i in above lemma to be $\|\nabla_{\theta} f(\mathbf{x}_i, \theta^*)\|_F^2$ and let $p = 1, q = k/2$, then we get

$$\left(\sum_{i=1}^n (\|\nabla_{\theta} f(\mathbf{x}_i, \theta^*)\|_F^2)^{k/2} \right)^{2/k} \leq \sum_{i=1}^n \|\nabla_{\theta} f(\mathbf{x}_i, \theta^*)\|_F^2. \quad (20)$$

Therefore,

$$\begin{aligned} \frac{\|\mathbf{W}\|_F^k}{\min_i \|\mathbf{x}_i\|_2^k} \frac{1}{n} \sum_{i=1}^n \|\nabla_{\theta} f(\mathbf{x}_i, \theta^*)\|_F^k &\leq \frac{n^{k/2-1} \|\mathbf{W}\|_F^k}{\min_i \|\mathbf{x}_i\|_2^k} \left(\frac{1}{n} \sum_{i=1}^n \|\nabla_{\theta} f(\mathbf{x}_i, \theta^*)\|_F^2 \right)^{k/2} \\ &= \frac{n^{k/2-1} \|\mathbf{W}\|_F^k}{\min_i \|\mathbf{x}_i\|_2^k} S(\theta^*)^{k/2} \end{aligned} \quad (21)$$

Case 2: $1 \leq k < 2$

Lemma B.2. For vector $\mathbf{x} \in \mathbb{R}^n$, $\|\mathbf{x}\|_p \leq n^{1/p-1/q} \|\mathbf{x}\|_q$ for $1 \leq p \leq q \leq \infty$.

Proof. By Hölder's inequality, we have,

$$\sum_i |x_i|^p = \sum_i |x_i|^p \cdot 1 \leq \left(\sum_i |x_i|^q \right)^{p/q} \left(\sum_i 1 \right)^{1-p/q} = n^{1-p/q} \|\mathbf{x}\|_q^p \quad (22)$$

Taking the p -th root on both sides gives us the desired inequality. □

Now take the x_i in above lemma to be $\|\nabla_{\theta} f(\mathbf{x}_i, \theta^*)\|_F$ and let $p = k, q = 2$, then we get

$$\left(\sum_{i=1}^n (\|\nabla_{\theta} f_i\|_F)^k \right)^{1/k} \leq n^{1/k-1/2} \left(\sum_{i=1}^n \|\nabla_{\theta} f_i\|_F^2 \right)^{1/2}. \quad (23)$$

Therefore,

$$\begin{aligned} \frac{\|\mathbf{W}\|_F^k}{\min_i \|\mathbf{x}_i\|_2^k} \frac{1}{n} \sum_{i=1}^n \|\nabla_{\theta} f_i\|_F^k &\leq \frac{\|\mathbf{W}\|_F^k}{\min_i \|\mathbf{x}_i\|_2^k} \frac{n^{1-k/2}}{n} \left(\sum_{i=1}^n \|\nabla_{\theta} f_i\|_F^2 \right)^{k/2} \\ &= \frac{\|\mathbf{W}\|_F^k}{\min_i \|\mathbf{x}_i\|_2^k} S(\theta^*)^{k/2}. \end{aligned} \quad (24)$$

Combining Eq. (21) and Eq. (24), we get Eq. (12).

C PROOF OF EQ. (13)

From Eq. (5), we get

$$\overline{\text{MLS}} = \frac{1}{n} \sum_{i=1}^n \|\nabla_{\mathbf{x}} f_i\|_2 \leq \|\mathbf{W}\|_2 \frac{1}{n} \sum_{i=1}^n \frac{\|\nabla_{\mathbf{w}} f(\mathbf{x}_i, \boldsymbol{\theta}^*)\|_F}{\|\mathbf{x}_i\|_2}. \quad (25)$$

Now the Cauchy-Schwarz inequality tells us that

$$\left(\sum_{i=1}^n \frac{\|\nabla_{\mathbf{w}} f_i\|}{\|\mathbf{x}_i\|_2} \right)^2 \leq \left(\sum_{i=1}^n \frac{1}{\|\mathbf{x}_i\|_2^2} \right) \cdot \left(\sum_{i=1}^n \|\nabla_{\mathbf{w}} f_i\|^2 \right). \quad (26)$$

Therefore

$$\begin{aligned} \overline{\text{MLS}} &\leq \|\mathbf{W}\|_2 \sqrt{\frac{1}{n} \sum_{i=1}^n \frac{1}{\|\mathbf{x}_i\|_2^2}} \cdot \sqrt{\frac{1}{n} \sum_{i=1}^n \|\nabla_{\mathbf{w}} f_i\|^2} \\ &\leq \|\mathbf{W}\|_2 \sqrt{\frac{1}{n} \sum_{i=1}^n \frac{1}{\|\mathbf{x}_i\|_2^2}} \cdot S(\boldsymbol{\theta}^*)^{1/2}. \end{aligned} \quad (27)$$

D EMPIRICAL ANALYSIS OF THE BOUND

D.1 TIGHTNESS OF THE BOUND

In this section, we mainly explore the tightness of the bound in Eq. (13) for reasons discussed in Sec. 3.2. First we rewrite Eq. (13) as

$$\begin{aligned} \overline{\text{MLS}} &= \frac{1}{n} \sum_{i=1}^n \|\nabla_{\mathbf{x}} f(\mathbf{x}_i, \boldsymbol{\theta}^*)\|_2 && := A \\ &\leq \frac{\|\mathbf{W}\|_2}{n} \sum_{i=1}^n \frac{\|\nabla_{\mathbf{w}} f(\mathbf{x}_i, \boldsymbol{\theta}^*)\|_F}{\|\mathbf{x}_i\|_2} && := B \\ &\leq \|\mathbf{W}\|_2 \sqrt{\frac{1}{n} \sum_{i=1}^n \frac{1}{\|\mathbf{x}_i\|_2^2}} \sqrt{\frac{1}{n} \sum_{i=1}^n \|\nabla_{\mathbf{w}} f(\mathbf{x}_i, \boldsymbol{\theta}^*)\|_F^2} && := C \\ &\leq \|\mathbf{W}\|_2 \sqrt{\frac{1}{n} \sum_{i=1}^n \frac{1}{\|\mathbf{x}_i\|_2^2}} S(\boldsymbol{\theta}^*)^{1/2} && := D \end{aligned} \quad (28)$$

Thus Eq. (13) consists of 3 different steps of relaxations. We analyze them one by one:

1. ($A \leq B$) The equality holds when $\|W^T J\|_2 = \|W\|_2 \|J\|_2$ and $\|J\|_F = \|J\|_2$, where $J = \frac{\partial f(\mathbf{W}\mathbf{x}; \boldsymbol{\theta})}{\partial(\mathbf{W}\mathbf{x})}$. The former equality requires that W and J have the same left singular vectors. The latter requires J to have zero singular values except for the largest singular value. Since J depends on the specific neural network architecture and training process, we test the tightness of this bound empirically (Fig. D.4).
2. ($B \leq C$) The equality requires $\frac{\|\nabla_{\mathbf{w}} f(\mathbf{x}_i, \boldsymbol{\theta}^*)\|_F}{\|\mathbf{x}_i\|_2}$ to be the same for all i . In other words, the bound is tight when $\frac{\|\nabla_{\mathbf{w}} f(\mathbf{x}_i, \boldsymbol{\theta}^*)\|_F}{\|\mathbf{x}_i\|_2}$ does not vary too much from sample to sample.
3. ($C \leq D$) The equality holds if the model is linear, i.e. $\boldsymbol{\theta} = \mathbf{W}$.

We empirically verify the tightness of the above bounds in Fig. D.4

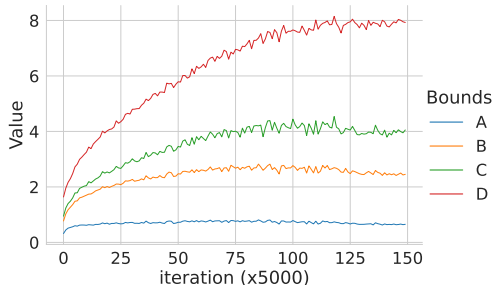


Figure D.4: **Empirical tightness of the bounds.** We empirically verify that the inequalities in Eq. (28) hold and test their tightness. The results are shown for a fully connected feedforward network trained on the FashionMNIST dataset. The quantities A, B, C, and D are defined in Eq. (28). We see that the gap between C and D is large compared to the gap between A and B or B and C. This indicates that partial sharpness $\|\nabla_{\mathbf{W}} f(\mathbf{x}_i, \boldsymbol{\theta}^*)\|_F$ (sensitivity of the loss w.r.t. only the input weights) is more indicative of the change in the maximum local sensitivity (A). Indeed, correlation analysis shows that bound C is positively correlated with MLS while bound D, perhaps surprisingly, is negatively correlated with MLS (Fig. D.6).

D.2 CORRELATION ANALYSIS

We empirically show how different metrics correlate with each other, and how these correlations can be predicted from our bounds. We train 20 VGG10 networks with different batch sizes, learning rates, and random initialization to classify images from the CIFAR-10 dataset, and plot pairwise scatter plots between 5 quantities at the end of the training: test loss, MLS, G (see Eq. (6)), log volume, sharpness and local dimensionality (Fig. D.5).

We find that

1. G and MLS are highly correlated and can be almost seen as the same quantity, scaled.
2. Although the bound in Eq. (12) is loose, log volume correlates well with sharpness and MLS.
3. Sharpness is positively correlated with the test loss, indicating that little reparametrization effect (Dinh et al., 2017) is happening during training, i.e. the network weights do not change too much during training. This is consistent with observations in Ma & Ying (2021).
4. MLS improves the correlation with the test loss over log volume and local dimensionality. This is consistent with the bound Eq. (13).

We repeat the analysis on an MLP trained on the FashionMNIST dataset, and observe the same phenomena (Fig. D.6).

D.3 CONNECTION TO OTHER WORKS

Our bound and its analysis are connected to many theoretical and experimental results. First of all, the right-hand side of Eq. (13) is related not only to the sharpness but also to the norm of the input weights. Therefore our bound takes into the effect of reparametrization, and is invariant under scaling of the input weights. This is consistent with the theoretical results in Dinh et al. (2017) which show that sharpness can be arbitrarily increased by reparametrization while the network can still generalize. Moreover, many works studied simplified linear models (Li et al., 2022; Ding et al., 2023; Nacson et al., 2022; Gatmiry et al., 2023), and showed that the flattest minima generalize well. Correspondingly, Eq. (28) shows that when the neural network is linear, the inequality between C and D becomes equality, and the flattest minima give the tightest bound on MLS. On the other hand, this also explains why sharpness does not always correlate with generalization when the network becomes more complicated (Wen et al., 2023; Andriushchenko et al., 2023): having weights that are other than the input weights makes the bound looser and more unpredictable. Experiments on

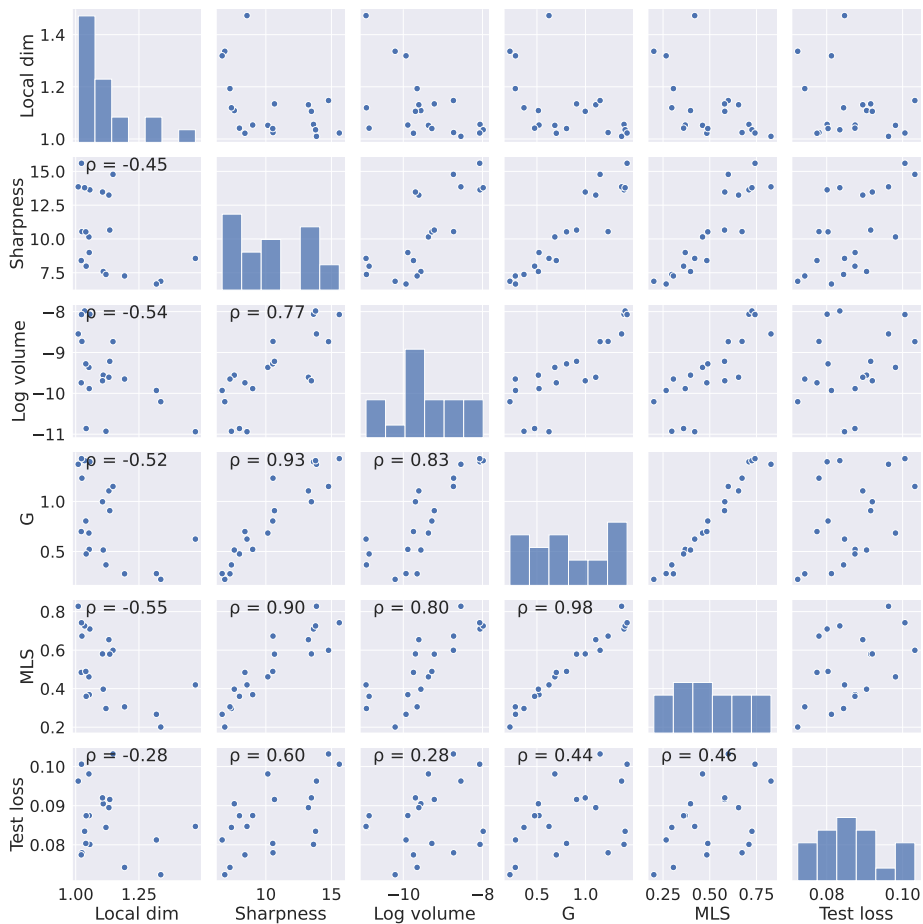


Figure D.5: **Pairwise correlation among different metrics.** We trained 20 different VGG10 networks using vanilla SGD with different learning rates, batch sizes, and random initializations and plot pairwise scatter plots between different quantities: local dimensionality, sharpness (square root of Eq. (3)), log volume (Eq. (10)), G (Eq. (6)), MLS (Eq. (13)) and test loss. The Pearson correlation coefficient ρ is shown in the top-left corner for each pair of quantities. See Appendix D.2 for a summary of the findings in this figure.

MLP show that the bound D in Eq. (28) can even be negatively correlated with MLS and test loss (Fig. D.6).

E ADDITIONAL EXPERIMENTS

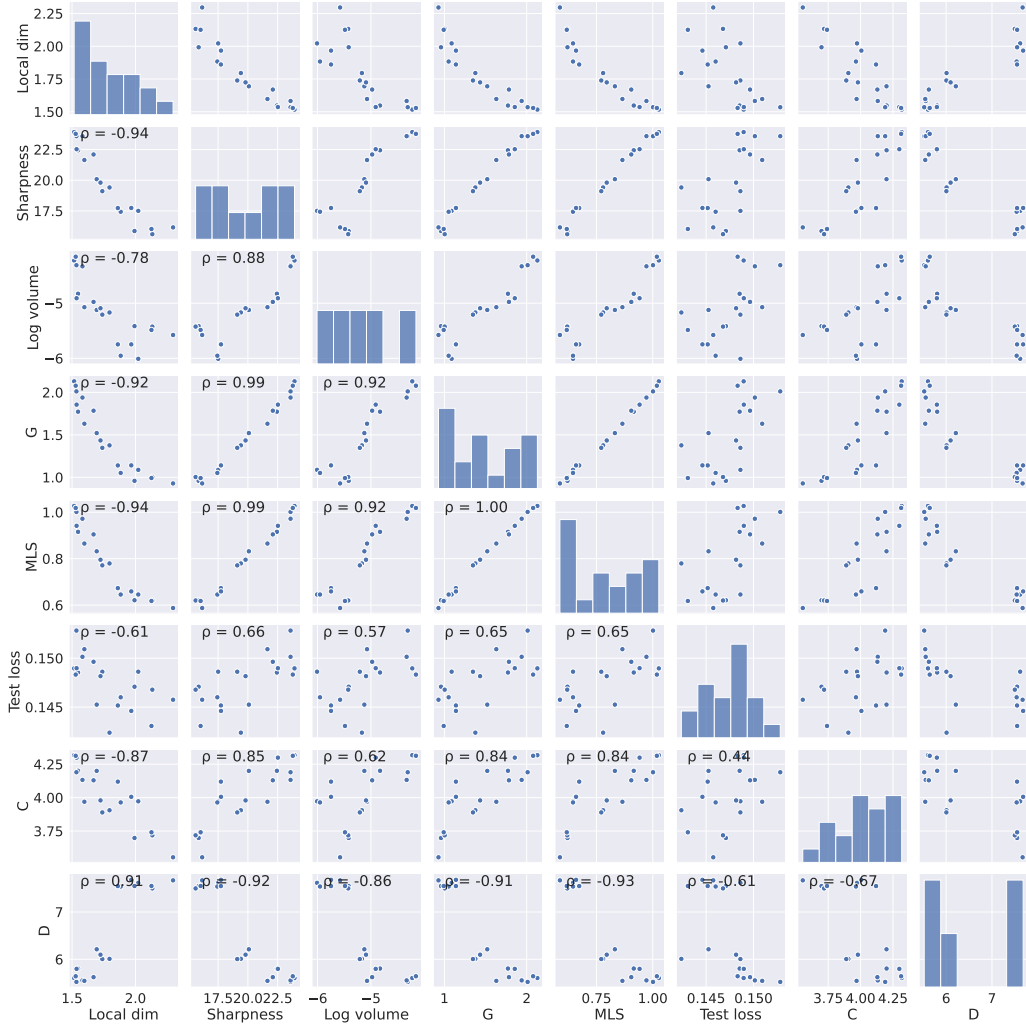


Figure D.6: **Pairwise correlation among different metrics.** We trained 20 different 4-layer MLPs using vanilla SGD with different learning rates, batch size, and random initializations and plot pairwise scatter plots between different quantities: local dimensionality, sharpness (square root of Eq. (3)), log volume (Eq. (10)), G (Eq. (6)), MLS (Eq. (13)), test loss and additionally bound C and D as defined in Eq. (28). The Pearson correlation coefficient ρ is shown in the top-left corner for each pair of quantities. See Appendix D.2 for a summary of the findings in this figure.

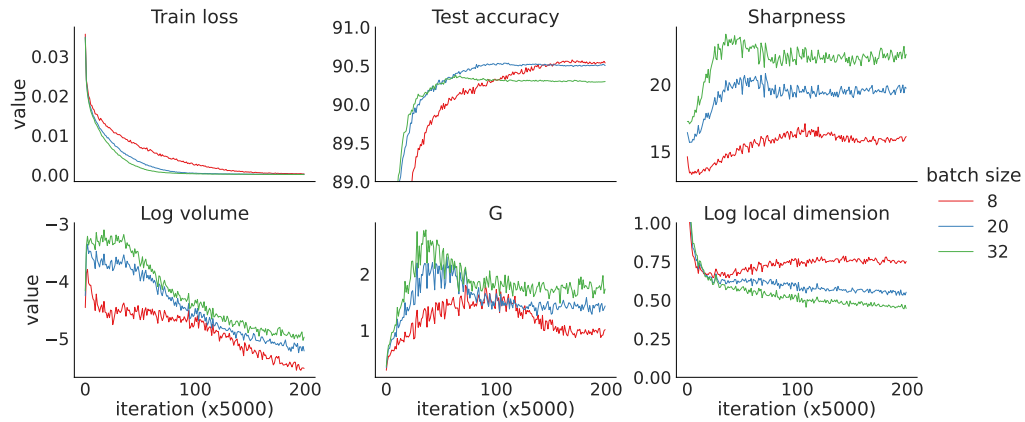


Figure E.7: Trends in key variables across SGD training of a 4-layer MLP with fixed learning rate (equal to 0.1) and varying batch size (8, 20, and 32). After minimizing the loss, lower batch sizes lead to lower sharpness and stronger compression. Moreover, G closely follows the trend of sharpness during the training. From left to right: train loss, test accuracy, sharpness (square root of Eq. (3)), log volumetric ratio (Eq. (10)), G (Eq. (6)), and local dimensionality of the network output (Eq. (14)).

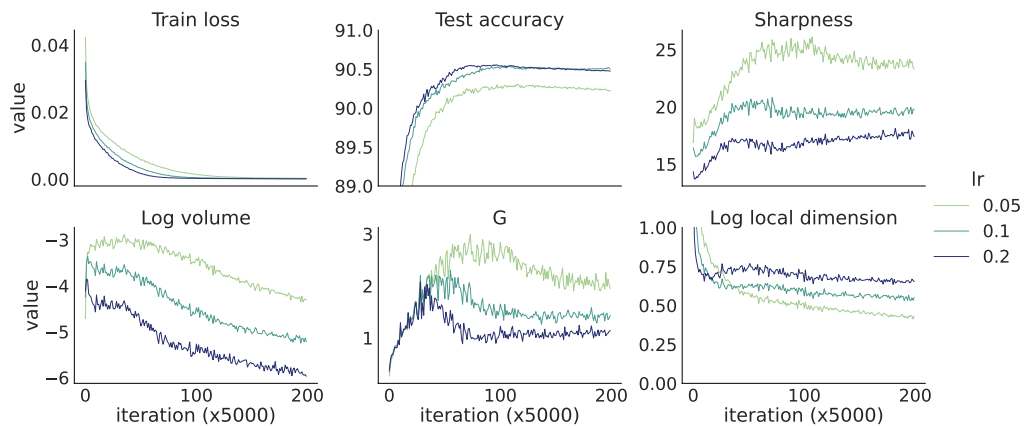


Figure E.8: Trends in key variables across SGD training of a 4-layer MLP with fixed batch size (equal to 20) and varying learning rates (0.05, 0.1 and 0.2). After the loss is minimized, higher learning rates lead to lower sharpness and hence stronger compression. Moreover, G closely follows the trend of sharpness during the training. From left to right: train loss, test accuracy, sharpness (square root of Eq. (3)), log volumetric ratio (Eq. (10)), G (Eq. (6)), and local dimensionality of the network output (Eq. (14)).